Enhanced Tidal Intrusion in the Barataria Basin, Mississippi River Delta

Authors: Kang, Byungho, and Xie, Surui

Source: Journal of Coastal Research, 41(2) : 336-346

Published By: Coastal Education and Research Foundation

URL: https://doi.org/10.2112/JCOASTRES-D-24-00047.1

Journal of Coastal Research	41	2	336–346	Charlotte, North Carolina	March 2025

Enhanced Tidal Intrusion in the Barataria Basin, Mississippi River Delta

Byungho Kang[†‡*] **and Surui Xie**[†‡]

[†]Department of Civil and Environmental Engineering
University of Houston
Houston, TX 77204, U.S.A.

www.cerf-jcr.org

www.JCRonline.org

ABSTRACT

Kang, B. and Xie, S., 2025. Enhanced tidal intrusion in the Barataria Basin, Mississippi River Delta. *Journal of Coastal Research,* 41(2), 336–346. Charlotte (North Carolina), ISSN 0749-0208.

Microtidal deltaic systems, comprising a significant portion of global coastal wetlands, are increasingly vulnerable to the combined effects of accelerated sea-level rise and anthropogenic modifications. This study investigates two decades of tidal propagation trends within Louisiana's Barataria Basin, a representative microtidal delta, using wavelet analysis and cross-spectrum techniques applied to a long-term water-level dataset. Results showed a consistent decrease in the predominant (K1) tidal constituent's attenuation, with amplitude ratios at inland stations increasing by as much as 50% between 2008 and 2022. Furthermore, analysis of tidal phase lag variations indicates an increasing trend in K1 tidal wave celerity, suggesting more efficient inland propagation of diurnal tide. This study highlights the rapidly evolving tidal dynamics in microtidal systems and demonstrates the utility of wavelet-based approaches for quantifying these critical changes.

ADDITIONAL INDEX WORDS: *Tidal propagation, sea level changes, coastal vulnerability, wavelet analysis, microtidal deltas.*

INTRODUCTION

Coastal wetlands, among the Earth's most biologically productive ecosystems, are facing unprecedented threats from rising seas and human activities. These threats are particularly severe in microtidal deltaic systems, which comprise a substantial portion of global coastal wetlands and are sensitive to sea-level rise and human modifications.

Examining the effects of sea-level rise on coastal wetlands requires a quantitative understanding of how specific deltaic systems respond. The well-instrumented Mississippi River Delta (MRD) in coastal Louisiana provides a critical case study, offering valuable insights into the challenges facing microtidal deltas worldwide. Over the past century, the MRD has experienced significant land loss due to land subsidence, sea-level rise, and reduced sediment input (Blum and Roberts, 2009; Törnqvist *et al.*, 2020). This loss is exacerbated by levee construction, which alters sediment dynamics and can lead to further subsidence (Edmonds *et al.*, 2023; Keogh *et al.*, 2021; Sanks, Shaw, and Naithani, 2020).

The MRD's low elevation and ongoing land loss make it exceptionally vulnerable to sea-level rise and tidal dynamics. Tides play a crucial role in estuarine health, influencing flushing capacity and the transport of nutrients and sediments (Kirwan and Murray, 2007; Monsen *et al.*, 2002). However, sea-level rise and amplification in tidal range can exacerbate coastal flooding, a growing concern in low-lying areas such as the Barataria Basin, which is already experiencing these impacts (Couvillion *et al.*, 2017; Day *et al.*, 2021; Payandeh *et al.*, 2022).

Prior studies have shown a strong link between tidal amplification and the increasing frequency of nuisance flooding events along coastlines, a trend projected to intensify in coming decades (Balke *et al.*, 2016; Li *et al.*, 2021; Thompson *et al.*, 2021). The response of estuaries to sea-level rise is size dependent, with small, shallow estuaries being particularly susceptible to tidal amplification and flood risk (Leuven *et al.*, 2019). This highlights the significance of investigating tidal propagation trends in microtidal deltaic systems.

While astronomical forcings are fundamental drivers of tidal dynamics, non-astronomical factors, including ocean stratification, river discharge, and human modifications to estuaries (*e.g.*, dredging, land reclamation), can considerably influence tidal patterns and propagation (Devlin *et al.*, 2014; Moftakhari *et al.*, 2013; Savenije *et al.*, 2008; Talke and Jay, 2020; Winterwerp and Wang, 2013). Sea-level rise will further exacerbate these complexities (Masson-Delmotte *et al.*, 2021). Although numerical models offer valuable insights into potential changes in tidal patterns under various sea-level rise scenarios, they often rely on simplified representations of these complex coastal systems, limiting their accuracy and predictive power (Cai, Savenije, and Toffolon, 2012; Du *et al.*, 2018; Eslami *et al.*, 2019; Holleman and Stacey, 2014; Lee, Li, and Zhang, 2017; Li, Huang, and Milan, 2019; Pickering *et al.*, 2012; Toffolon and Savenije, 2011).

To address this need for an in-depth understanding, this study investigates tidal propagation trends within the Barataria Basin over the past two decades. Using a novel application of wavelet analysis on a comprehensive dataset from the Coastwide Reference Monitoring System (CRMS), this research examines changes in the magnitude and celerity of the dominant

DOI: 10.2112/JCOASTRES-D-24-00047.1 received 2 July 2024; accepted in revision 21 August 2024; corrected proofs received 3 November 2024; published pre-print online 27 November 2024.
*Corresponding author: byunghokang@kmou.ac.kr
[‡]Present address: Division of Navigation Convergence, National Korea Maritime and Ocean University, Busan, 49112, Republic of Korea.

tidal constituent (K1) as it propagates inland. This method enables a detailed examination of nonstationary signals, such as tidal fluctuations, that vary over time. Wavelet analysis has been successfully applied to river-tide interactions (Jay *et al*., 2015; Leonardi, Kolker, and Fagherazzi, 2015; Spicer *et al*., 2019), but its potential for quantifying tidal celerity in dynamic wetland environments remains underutilized (Nordio and Fagherazzi, 2022). Specifically, this study leverages wavelet analysis to estimate tidal celerity changes in wetlands, a key indicator of evolving tidal dynamics.

METHODS

This study relies on a robust dataset and a wavelet analysis method to investigate the evolving tidal dynamics of the Barataria Basin. Water-level data from multiple sources were acquired and carefully processed to ensure quality and consistency.

Environmental Setting

The Barataria Basin, spanning approximately 7100 km^2 within coastal Louisiana's northern Gulf of Mexico, is a typical microtidal deltaic system threatened by accelerated sea-level rise and human influences (Byrnes *et al*., 2019; Day *et al*., 2007). The diverse landscape—featuring marshes, bayous, lakes, and barrier islands—experiences significant land loss because of subsidence, reduced sediment input, and sea-level rise, making it particularly susceptible to changes in tidal dynamics (Das *et al.*, 2012). The Barataria Basin is directly connected to the Gulf of Mexico through tidal inlets, such as Caminada Pass and Barataria Pass. This facilitates dynamic exchanges of water, sediment, and nutrients (Snedden, 2006; Figure 1a). Understanding how tides vary spatially and temporally in this system is essential for assessing its vulnerability to nuisance flooding and the effectiveness of restoration efforts. The basin exhibits microtidal conditions with diurnal tidal dynamics, primarily driven by the K1 and O1 tidal constituents (Sorourian *et al.*, 2020). The tidal ranges experience significant attenuation as tides move landward (Ou *et al*., 2020; Payandeh *et al*., 2022).

Data and Preprocessing

To investigate the long-term trends of tidal propagation patterns, the study incorporates water-level observations from the Grand Isle tidal gauge (National Oceanic and Atmospheric Administration [NOAA] station ID: 8761724) and the network of monitoring gauges established by the CRMS (Figure 1a). The hourly water height measurements from the Grand Isle tidal gauge were used to quantify ocean tidal variations, establishing a baseline for comparison with inland stations. Located near the entrance of Barataria Bay (29.263°N, 89.957°W), the gauge provides a representative measure of the tides entering the basin. Quality-controlled records from 1981–2022 were used for this study. A relative sea-level rise rate of 8.3 mm/y was calculated at this location, which was used for detrending (Figure 1b). This rate is slightly slower than the 9.16 ± 0.37 mm/y, local sea-level trend averaged from 1947 to 2022 by NOAA. The difference likely arises from different time spans and possible differences in vertical land movement rates over time.

To analyze local water-level changes within the Barataria Basin, hourly water elevation data from 49 CRMS stations located at salt marshes near Barataria Bay were used (Figure 1a). These stations are distributed along the landward progression of tidal influence, which allow tracking of the attenuation of tidal heights as they move inland, providing information on the spatial variability of tidal dynamics within the basin. The CRMS water-level data were preprocessed to ensure quality and consistency (CPRA, 2022), including correction from biofouling and instrumental drift and elimination of erroneous data. As the height datum of the raw data transitioned from the GEOID99 model to the GEOID12A model in 2013, a correction was applied to reference all data to the GEOID12A model for consistency.

Because of the scarcity of earlier studies on regional sea-level rise rates (Jankowski, Tornqvist, and Fernandes, 2017), CRMS data were detrended using a rate of 3 mm/y to reflect the contribution of geocentric sea-level rise. This rate is consistent with global sea-level rise estimates ranging from 3.0 mm/y (Nerem *et al.*, 2018) to 3.6 mm/y (Masson-Delmotte *et al.*, 2021), although it is slightly higher than the historical rate in the Gulf of Mexico, which has been reported to be lower than the global average because of regional ocean dynamics and land ice melt contributions (Sweet *et al.*, 2017). On the other hand, distances to the coastline for each station represent the cross-track distances between each CRMS station and a reference line connecting two points (29.1136°N, 90.1498°W and 29.4296°N, 89.6180°W), calculated using the Haversine formula.

Wavelet Analysis of Tidal Signal

Wavelet analysis is a well-established technique in signal processing, which can evaluate signal variations across time and frequency domains. The method allows a detailed understanding of nonstationary signals with time-varying frequency components, a significant advantage over Fourier methods (Torrence and Compo, 1998). This study uses generalized Morse wavelets to analyze tidal propagation pattern within the basin's complex network of water channels and bays. Generalized Morse wavelets allow precise estimation of both the amplitude and phase of nonstationary tidal signals (Olhede and Walden, 2002).

Considering the small range of variations in tidal amplitudes, this study focuses specifically on the K1 tidal constituent, which exhibits the highest signal-to-noise ratio based on tidal harmonic analysis. Wavelet analysis was conducted using 32 voices per octave, with smoothing performed over six consecutive scales. This approach identified the period for the K1 constituent as 23.90 hours, closely approximating the actual period of 23.93 hours. Given that this difference falls within the resolution limits set by the Rayleigh criterion, the wavelet coefficients for the 23.90-hour period can effectively serve as a proxy for the K1 constituent.

Tidal Amplitude Ratio Estimation Using Wavelet Spectrum

To quantify tidal attenuation at CRMS stations relative to the reference gauge at Grand Isle, the wavelet coefficients for the detrended water height time series for each station were calculated focusing on the K1 tidal constituent.

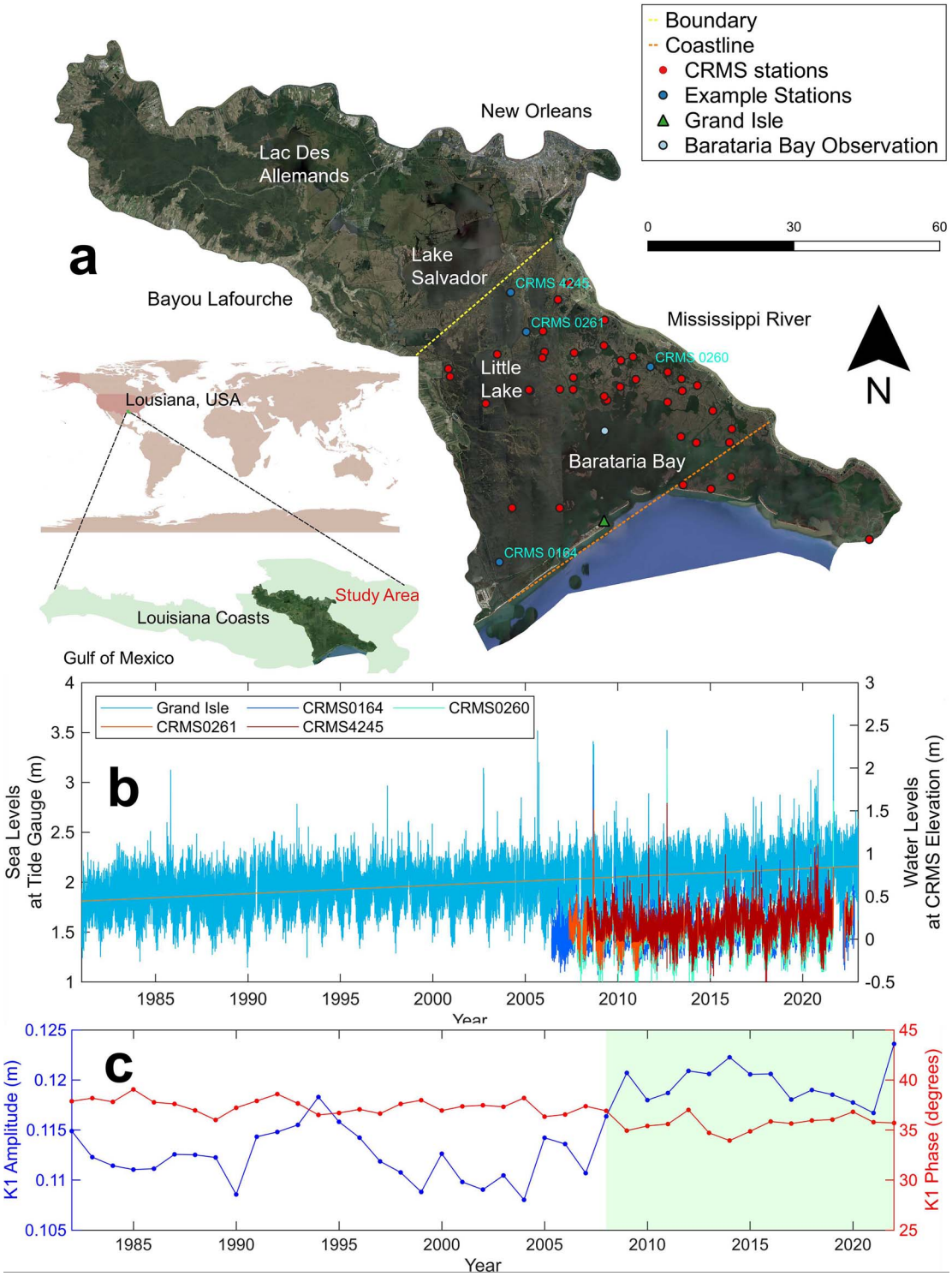

Figure 1. (a) Map of the study area within the Barataria Basin along the Louisiana coast. The dotted yellow line marks the boundary between the upper and lower Barataria. The dotted orange line is used as a reference to calculate the distances between Coastwide Reference Monitoring System (CRMS) stations and the coastline. (b) Time series of water elevation at the Grand Isle tidal station and selected CRMS Stations. The Grand Isle data are referenced to the station datum and reflect both geocentric sea-level rise and land subsidence. The CRMS data have instrument drift adjusted and are referenced to NAVD 88. (c) Time series of the annual amplitude (blue) and phase (red) of the K1 tidal constituent at Grand Isle from 1981 to 2022. The analysis was performed using the T-TIDE program (Pawlowicz, Beardsley, and Lentz, 2002), with a correction applied to account for the 18.6-year nodal cycle.

Wavelet coefficients for K1 tidal constituent for each station can be represented as $W_m(t_i)$, where m is the station index ranging from 1 to 49 and t_i denotes time (the ith hour). The same coefficients for the reference station at Grand Isle are denoted as $W_p(t_i)$. The tidal amplitude ratio $r_{mp}(t_i)$ was then calculated at each time t_i using the following equation:

$$r_{mp}(t_i) = \frac{|W_m|}{|W_p|}. \quad (1)$$

To determine the average attenuation rate across different time scales, both the monthly and annual means, along with the standard deviation of the ratio r_{mp}, were calculated. This involved using N_X, the number of hourly observations within the time scale X. In this context, $X = t$ corresponds to monthly time scales, with N_t representing the total number of hours in a month. Likewise, $X = T$ corresponds to annual time scales, with N_T representing the total hours in a year. Then, the mean ratio for a time scale X is calculated as:

$$\bar{r}(X) = \frac{1}{N_X}\sum_{i=1}^{N_X} r_{mp}(t_i) \quad (2)$$

The standard deviation for the time scale X is given by:

$$\sigma_{r_j}(X) = \sqrt{\frac{1}{N_X}\sum_{i=1}^{N_X}\left(r_{mp}(t_i) - \bar{r}(X)\right)^2} \quad (3)$$

On the other hand, to robustly measure the uncertainty of the yearly ratio $\bar{r}(T)$, the error was estimated using the bootstrapping method, performed 2000 times, along with the standard deviation.

Celerity Estimation Using Cross Spectrum

To better understand the time delays between diurnal signals at each CRMS station and Grand Isle, a cross-wavelet analysis was conducted. This approach involved calculating the cross-wavelet spectrum to determine the phase difference between two stations, as detailed in Equation (4):

$$W_{mp}(t_i) = S\left(W_m W_p^*\right) \quad (4)$$

where, * indicates complex conjugate, and S represents a smoothing operator. Next, the wavelet coherence $\gamma_{mp}(t_i)$ was calculated as a normalized measure of the cross-wavelet transforms:

$$\gamma_{mp}(t_i) = \frac{|S(W_{mp})|^2}{S\left(|W_m|^2\right)\cdot S\left(|W_p^*|^2\right)}. \quad (5)$$

Wavelet coherence values, ranging from 0 to 1, reflect the strength of covariance between the two signals, with higher values indicating stronger cross-correlations.

Using the cross-wavelet spectrum, the phase lag at time t_i:

$$\phi_{mp}(t_i) = arg\left(W_{mp}\right) \quad (6)$$

was examined between two time series. A phase lag of $\phi_{mp} \approx 0°$ suggests a synchronous relationship, *i.e.* the tidal peaks and troughs at both stations occur nearly simultaneously.

On the other hand, a phase lag of $\phi_{mp} \approx 180°$ indicates antiphase relationship. For both monthly and annual scales, the mean and standard deviation of the phase lag are computed by equations:

$$\bar{\phi}_j(X) = \frac{1}{N_X}\sum_{i=1}^{N_X}\phi_{mp}(t_i) \quad (7)$$

and

$$\sigma_{\phi_j}(X) = \sqrt{\frac{1}{N_X}\sum_{i=1}^{N_X}\left(\phi_{mp}(t_i) - \bar{\phi}_j(X)\right)^2} \quad (8)$$

For practical interpretation, phase lags were converted into time delays (lagged hours of signal propagation) using:

$$l_{mp}(X) = \bar{\phi}_j(X) \times \frac{1}{0.0418} \quad (9)$$

where $\bar{\phi}_j(X)$ is the mean phase angle computed over the period X. The constant 0.0418, reflecting the frequency of the K1 tidal constituent (cycles per hour), is used to convert the phase angle into time units.

Regression Analyses

To further quantify the spatial and temporal patterns of tidal propagation, regression analyses were employed. For the amplitude ratios, an exponential regression model of the form $y_1 = Ae^{-\alpha x}$ was used, where y_1 represents the amplitude ratio, A is a scaling constant, α is the attenuation coefficient (representing the rate of amplitude decay with distance), and x is the distance from the coastline (Figure 1a). Likewise, for the lagged hours, a linear regression model of the form $y_2 = 1/(\beta x)$ was used, where y_2 represents the lagged hours and β is the yearly celerity (representing the speed of tidal wave propagation).

RESULTS

Analysis of the long-term water-level records revealed significant changes in tidal propagation patterns within the Barataria Basin. Most notably, the attenuation of the dominant K1 tidal constituent exhibited distinct spatial and temporal variations, signaling a shift in how tidal influence is distributed across the basin. However, no significant trend is observed in either the amplitude or phase of the K1 constituent at Grand Isle (Figure 1c) from 2008 to 2022, suggesting that these changes within the Barataria Basin are primarily driven by internal factors rather than variations in the tidal forcing at the basin's entrance.

Attenuation Patterns

Analysis of the dominant K1 tidal constituent's monthly mean amplitude ratios across the basin's CRMS stations

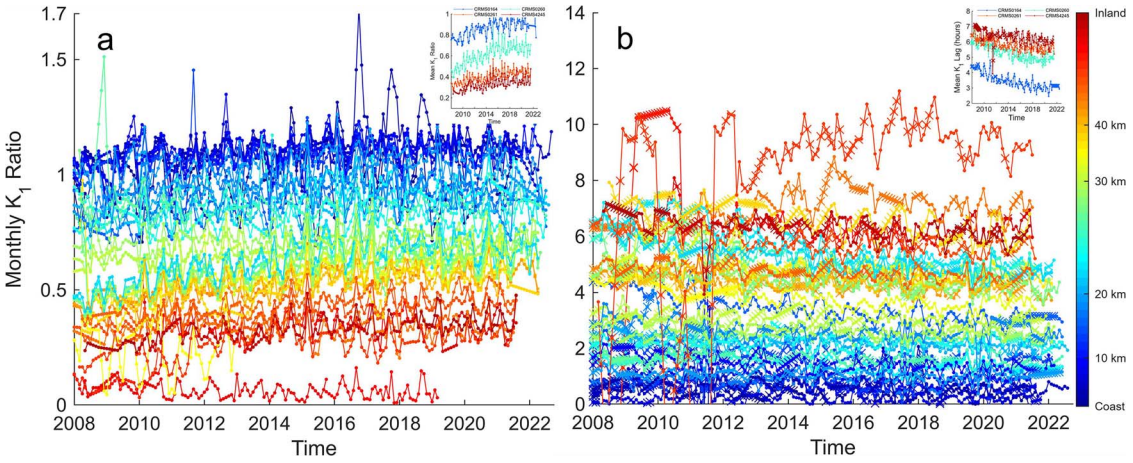

Figure 2. Monthly variations in (a) the amplitude ratio and (b) the time lag of K1 tidal constituents between the primary station (Grand Isle) and each Coastwide Reference Monitoring System (CRMS) station within the Southern Barataria Basin, spanning from January 2008 to December 2022. The blue-red color scheme represents the relative distance of each CRMS station from the nearest coastline segment (refer to Figure 1a for coastline depiction). Stations located on the seaward side of the coastline are assigned zero distance. The x symbols indicate data points that were linearly interpolated due to gaps in the original observations. (a) Interpolation was applied when the number of missing hourly observations within a month exceeded 48. (b) Interpolation was applied when the number of missing hourly observations within a month exceeded 48 or when the number of hours with wavelet coherence values less than 0.8 exceeded 80 hours, which ensures data continuity for analysis. The smaller plots within each panel highlight the monthly variations for specific example CRMS stations.

reveals spatial and temporal variations in tidal attenuation. The amplitude ratio is defined as the ratio between the tidal amplitude at a CRMS station and the reference station (*i.e.* the tide gauge at Grand Isle). Figure 2a shows a general trend: CRMS stations located near the coastline exhibit higher monthly K1 amplitude ratios compared with the inland stations. The monthly K1 amplitude ratios fluctuate between ~0.9 to 1.2 for coastal CRMS stations from 2008 to 2022, but they do not exhibit a clear temporal trend. In contrast, the K1 ratios for midbasin CRMS stations generally exhibit a distinct increasing trend (from 0.4–0.5 to 0.6 or greater). The ratios for inland CRMS stations show a generally increasing trend from ~0.2 in 2008 to 0.3–0.4 by 2022. Similar trends in K1 attenuation are observed using classical harmonic analysis, which presents a T-TIDE analysis of the Grand Isle and an example CRMS station for 2014–15 (Appendix Figure A1).

Over the studied period, the tidal ranges at CRMS stations near the coastline have generally increased (Figure 3a1–c1). Analysis of the tidal attenuation from 2009 to 2022 revealed a persistent decreasing trend in the attenuation coefficient for the K1 tidal constituent *vs.* distance, despite a temporary expansion of land area from 2009–16 (Figure 4). This trend remained consistent during the period from 2008–14, when nodal modulation led to a decline in diurnal tidal amplitudes. The southernmost region of the basin lies close to sea level (Figure 5a; digital elevation model), making it particularly sensitive to the combined effects of sea-level rise and the rapid subsidence exceeding 10 mm/y observed between 2007 and 2017 (Figure 5b).

Phase Lag and Tidal Wave Celerity

Analysis of the phase lag and celerity of diurnal tides between the CRMS stations and the reference tide gauge suggests that the tidal signals at coastal stations are nearly synchronized with the primary station at Grand Isle (Figure 2b). As the distance from the coastline increases, the lag time increases, although the relationship between distance and phase lag is not strictly linear. The temporal trend reflects a declining phase lag for the K1 tidal constituent across the CRMS stations (Figures 2–4).

The annual mean lag hours were calculated as a function of the distances to quantify how the phase lag evolves over time for the K1 tidal constituent between the reference station and CRMS stations (Figure 3a2–c2). Despite a significant noise level, the results show an increasing trend in tidal wave celerity (*i.e.* the inverse of the annual slope). Meanwhile, the standard deviations associated with the annual mean lag times exhibit intra-annual variability. Figure 4 shows the inverse of slopes depicted in Figure 3, illustrating a generally increasing trend in the yearly celerity of K1 tidal waves over time in the region.

DISCUSSION

The observed trends in tidal amplitude ratios within the Barataria Basin are consistent with patterns observed in other deltaic systems experiencing accelerated sea-level rise and human-induced subsidence. For example, Eslami *et al.* (2019) documented similar trends of tidal amplification and saltwater intrusion in the Mekong Delta, driven by anthropogenic sediment starvation. These studies highlight the vulnerability of microtidal coastal wetlands to shifts in hydrodynamic regimes driven by both global change and localized anthropogenic impacts.

As shown in Figure 2a, K1 amplitude ratios are generally increasing across the basin, particularly inland, suggesting the expanding influence of diurnal tides. The amplified tidal ranges

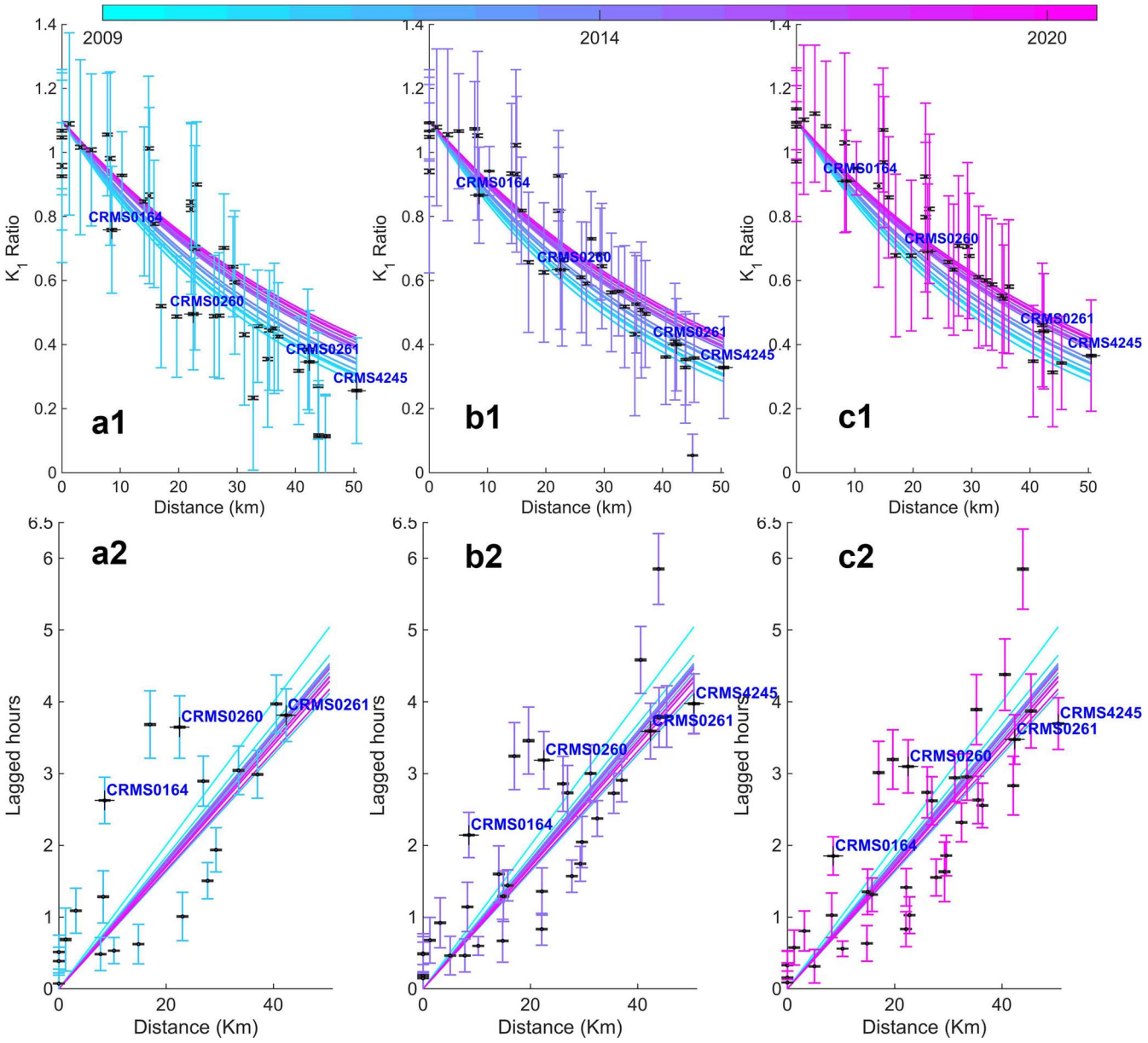

Figure 3. Annual mean K1 amplitude ratios (a1–c1) and lagged hours (a2–c2) *vs.* distance from the coastline for 2009 (left), 2014 (middle), and 2020 (right). (a1–c1) Ratio of the K1 tidal amplitude at each Coastwide Reference Monitoring System (CRMS) station to that at the primary tidal gauge at Grand Isle. Colored error bars represent the standard deviation, whereas dark gray error bars show the 95% confidence interval estimated via bootstrapping (2000 samples). The colored lines depict the exponential regression fit ($y_1 = 1.1e^{-\alpha x}$) highlighting the trend of decreasing amplitude ratio with distance, where α is the attenuation coefficient. Note: A linear fit does not improve the model. The + symbols mark the distance and ratio (a1–c1) or lagged hours (a2–c2) of example CRMS stations (names in blue text). (a2–c2) Mean time lag of the K1 tide at each CRMS station relative to the primary gauge. Error bars are as in (a1–c1). Colored lines illustrate the linear regression fit ($y_2 = 1/\beta x$), where β is the yearly celerity. The lines in both sets of panels (a1–c1 and a2–c2) are identical across the three years shown.

at coastal stations, with some amplitude ratios exceeding 1.1 (Figures 2a and 3a1–c1), can be attributed to factors such as nonlinear tidal distortion, water storage in intertidal zones, and the converging geometry of waterways (Friedrichs and Aubrey, 1988, 1994; Nidzieko, 2010; Savenije and Veling, 2005; Snedden, 2006; van Rijn, 2011). These empirical observations support the idea that small, shallow estuaries are particularly susceptible to tidal amplification (Leuven *et al.*, 2019).

The consistent trend of decreasing attenuation for the K1 tidal constituent, despite increase in land area (Figure 4), suggests that relative sea-level rise likely contributed to this trend (*e.g.*, by deepening tidal channels), although the relationship may be

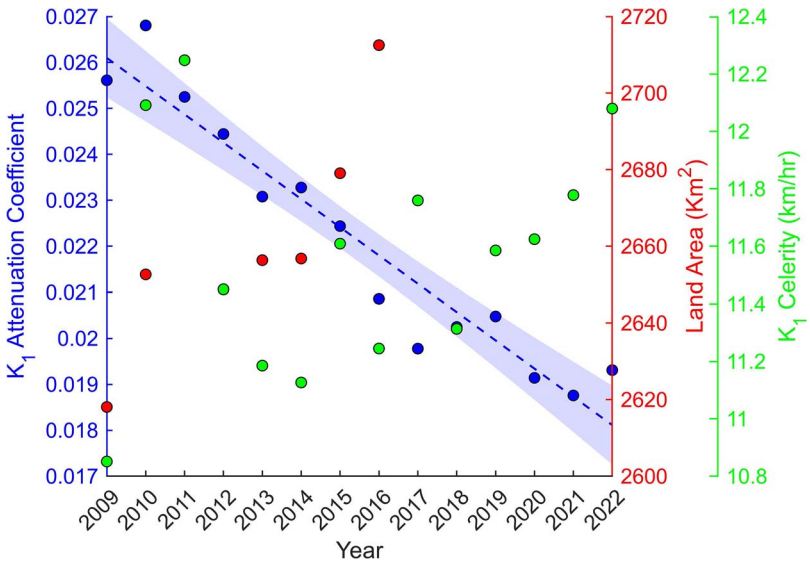

Figure 4. Trends in yearly mean K1 attenuation coefficients (α, blue circles) and celerity (β, green circles). Land area of the Barataria Basin (red circles, data from by Couvillion *et al.* [2017]) demonstrates an increasing trend, and K1 attenuation coefficients exhibit a statistically significant decreasing trend ($p < 0.001$; $R^2 = 0.77$). Meanwhile, K1 celerity shows a potentially increasing trend over time.

nonlinear (Appendix Figure A2; Pareja-Roman, Chant, and Sommerfield, 2020). The deepening could lead to a reduction in bottom friction, allowing for more efficient propagation of the tidal wave further inland. This deepening, along with the associated changes in salinity intrusion, could also influence vegetation patterns, which can further contribute to altered frictional effects within the basin (Stark *et al.*, 2015). Furthermore, high rates of land subsidence in the southernmost areas (Figure 5b), could lead to reorganization of waterways and the emergence of dominant channels, further enhancing tidal propagation (Sanks, Shaw, and Naithani, 2020; van Maren *et al.*, 2023). Quantifying the relative contributions of these factors to the observed K1 amplification requires further investigation using numerical tidal models, which can explicitly account for the interactions between sea level, bathymetry, and friction.

This trend of decreasing attenuation persisted even during the period from 2008–14, when the 18.6-year nodal cycle led to a decline in diurnal tidal amplitudes globally. However, the observed decrease in attenuation within the Barataria Basin during this period suggests that the effects of sea-level rise and changes in basin morphology are counteracting the

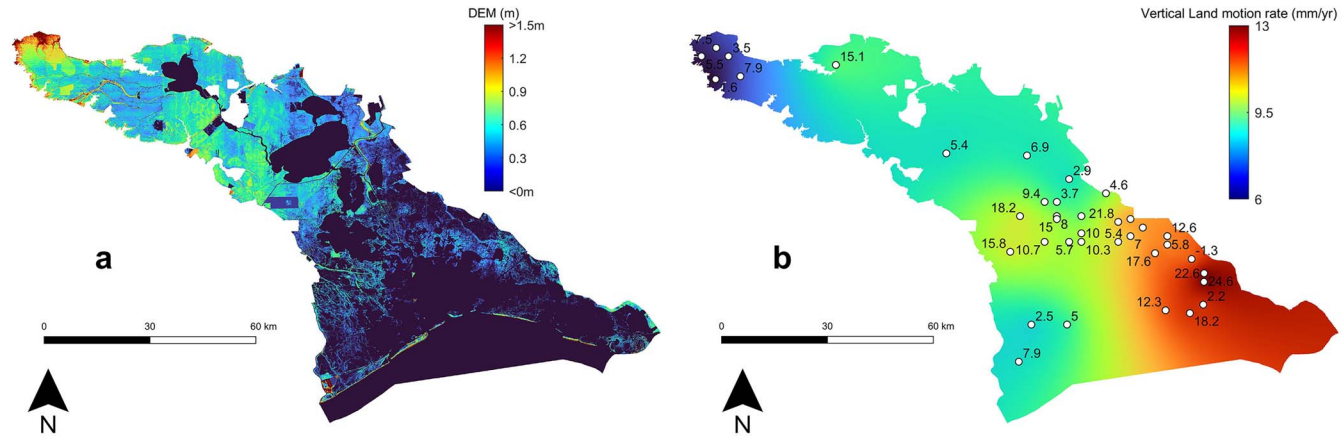

Figure 5. The digital elevation model and vertical land motion rates in the Barataria Basin. (a) Topobathymetric digital elevation models for the Barataria region (EROS, USGS, 2018). (b) Vertical land motion rates measurements (values shown next to points; data from Jankowski, Tornqvist, and Fernandes [2017]) and their Kriging-estimated spatial distribution (color map), using the interpolation method described in Nienhuis *et al.* (2017). Note that Kriging estimates may differ slightly from individual point measurements.

expected decrease in tidal amplitude because of the nodal cycle, implying that the increased tidal prism and altered bathymetry are enhancing tidal propagation inland and leading to larger tidal amplitudes further up the basin. The observed declining phase lag and increasing tidal wave celerity (Figures 2–4) further support this interpretation, indicating accelerated tidal propagation (Friedrichs and Aubrey, 1988; Savenije and Veling, 2005).

The observed changes in tidal propagation are not specific to a single tidal constituent but rather reflect a broader shift in the basin's hydrodynamic regime, potentially driven by factors such as changes in bathymetry, vegetation, or frictional effects. Such a shift could also have implications for the generation and behavior of overtides because changes in mean sea level and the amplitudes of primary tidal constituents can influence overtide dynamics. Further research investigating the evolution of overtides in response to these observed changes in tidal dynamics would be valuable.

CONCLUSIONS

Analysis of water-level data from the Barataria Basin's CRMS network (2008–22) reveals a clear trend of decreasing tidal attenuation and increasing celerity for the dominant K1 constituent. This indicates elevated tidal intrusion and improved efficiency in tidal propagation. These changes can lead to potentially significant consequences, including exacerbated saltwater intrusion and accelerated wetland loss. Although further research is needed to pinpoint the exact drivers, modifications in the basin's topobathymetry, driven by factors such as sediment transport and land subsidence, likely play a significant role. These findings highlight the increased vulnerability of microtidal deltaic systems to the compounding effects of climate change and human activities on coastal dynamics.

ACKNOWLEDGMENT

This research was supported by start-up funds from the University of Houston.

LITERATURE CITED

Balke, T.; Stock, M.; Jensen, K.; Bouma, T.J., and Kleyer, M., 2016. A global analysis of the seaward salt marsh extent: The importance of tidal range. *Water Resources Research*, 52, 3775–3786.

Blum, M.D. and Roberts, H.H., 2009. Drowning of the Mississippi Delta due to insufficient sediment supply and global sea-level rise. *Nature Geoscience*, 2, 488–491.

Byrnes, M.R.; Britsch, L.D.; Berlinghoff, J.L.; Johnson, R., and Khalil, S., 2019. Recent subsidence rates for Barataria Basin, Louisiana. *Geo-Marine Letters*, 39, 265–278.

Cai, H.; Savenije, H.H.G., and Toffolon, M., 2012. A new analytical framework for assessing the effect of sea-level rise and dredging on tidal damping in estuaries. *Journal of Geophysical Research: Oceans*, 117, C09023, 20 p.

Couvillion, B.R.; Beck, H.; Schoolmaster, D., and Fischer, M., 2017. *Land area change in coastal Louisiana (1932 to 2016)*. Reston, VA: Scientific Investigations Map.

Das, A.; Justic, D.; Inoue, M.; Hoda, A.; Huang, H., and Park, D., 2012. Impacts of Mississippi River diversions on salinity gradients in a deltaic Louisiana estuary: Ecological and management implications. *Estuarine, Coastal and Shelf Science*, 111, 17–26.

Day, J.W.; Boesch, D.F.; Clairain, E.J.; Kemp, G.P.; Laska, S.B.; Mitsch, W.J.; Orth, K.; Mashriqui, H.; Reed, D.J.; Shabman, L.; Simenstad, C.A.; Streever, B.J.; Twilley, R.R.; Watson, C.C.; Wells, J.T., and Whigham, D.F., 2007. Restoration of the Mississippi Delta: Lessons from Hurricanes Katrina and Rita. *Science*, 315, 1679–1684.

Day, J.W.; Conner, W.H.; DeLaune, R.D.; Hopkinson, C.S.; Hunter, R.G.; Shaffer, G.P.; Kandalepas, D.; Keim, R.F.; Kemp, G.P.; Lane, R.R.; Rivera-Monroy, V.H.; Sasser, C.E.; White, J.R., and Vargas-Lopez, I.A., 2021. A review of 50 years of study of hydrology, wetland dynamics, aquatic metabolism, water quality and trophic status, and nutrient biogeochemistry in the Barataria Basin, Mississippi Delta—System functioning, human impacts and restoration approaches. *Water*, 13(5), 642.

Devlin, A.T.; Jay, D.A.; Talke, S.A., and Zaron, E., 2014. Can tidal perturbations associated with sea level variations in the western Pacific Ocean be used to understand future effects of tidal evolution? *Ocean Dynamics*, 64, 1093–1120.

Du, J.; Shen, J.; Zhang, Y.J.; Ye, F.; Liu, Z.; Wang, Z.; Wang, Y.P.; Yu, X.; Sisson, M., and Wang, H.V., 2018. Tidal response to sea-level rise in different types of estuaries: The importance of length, bathymetry, and geometry. *Geophysical Research Letters*, 45, Issue 1, 227–235.

Earth Resources Observation and Science (EROS) Center, U.S. Geological Survey (USGS), 2018. *USGS EROS Archive - Digital Elevation - Coastal National Elevation Database (CoNED) Project - Topobathymetric Digital Elevation Model (TBDEM)*. https://www.usgs.gov/centers/eros/science/usgs-eros-archive-digital-elevation-coastal-national-elevation-database-coned

Edmonds, D.A.; Toby, S.C.; Siverd, C.G.; Twilley, R.; Bentley, S.J.; Hagen, S., and Xu, K., 2023. Land loss due to human-altered sediment budget in the Mississippi River Delta. *Nature Sustainability*, 6, 644–651.

Eslami, S.; Hoekstra, P.; Nguyen Trung, N.; Ahmed Kantoush, S.; Van Binh, D.; Duc Dung, D.; Tran Quang, T., and van der Vegt, M., 2019. Tidal amplification and salt intrusion in the Mekong Delta driven by anthropogenic sediment starvation. *Scientific Reports*, 9, 18746.

Friedrichs, C.T. and Aubrey, D.G., 1988. Non-linear tidal distortion in shallow well-mixed estuaries: A synthesis. *Estuarine, Coastal and Shelf Science*, 27, 521–545.

Friedrichs, C.T. and Aubrey, D.G., 1994. Tidal propagation in strongly convergent channels. *Journal of Geophysical Research: Oceans*, 99, 3321–3336.

Holleman, R.C. and Stacey, M.T., 2014. Coupling of sea level rise, tidal amplification, and inundation. *Journal of Physical Oceanography*, 44, 1439–1455.

IPCC, 2021. Summary for policymakers. *In* Masson-Delmotte, V.P.; Zhai, P.; Pirani, S.L.; Connors, C.; Péan, S.; Berger, N.; Caud, Y.; Chen, L.; Goldfarb, M.I., and Scheel Monteiro, P.M. (eds), Climate Change 2021: The Physical Science Basis. Contribution of Working Group I to the Sixth Assessment Report of the Intergovernmental Panel on Climate Change, 2(1), 2391.

Jankowski, K.L.; Tornqvist, T.E., and Fernandes, A.M., 2017. Vulnerability of Louisiana's coastal wetlands to present-day rates of relative sea-level rise. *Nature Communications*, 8, 14792.

Jay, D.A.; Leffler, K.; Diefenderfer, H.L., and Borde, A.B., 2015. Tidal-fluvial and estuarine processes in the lower Columbia River: I. Along-channel water level variations, Pacific Ocean to Bonneville Dam. *Estuaries and Coasts*, 38, 415–433.

Keogh, M.E.; Törnqvist, T.E.; Kolker, A.S.; Erkens, G., and Bridgeman, J.G., 2021. Organic matter accretion, shallow subsidence, and river delta sustainability. *Journal of Geophysical Research: Earth Surface*, 126, e2021JF006231.

Kirwan, M.L. and Murray, A.B., 2007. A coupled geomorphic and ecological model of tidal marsh evolution. *Proceedings of the National Academy of Sciences*, 104, 6118–6122.

Lee, S.B.; Li, M., and Zhang, F., 2017. Impact of sea level rise on tidal range in Chesapeake and Delaware Bays. *Journal of Geophysical Research: Oceans*, 122, 3917–3938.

Leonardi, N.; Kolker, A.S., and Fagherazzi, S., 2015. Interplay between river discharge and tides in a delta distributary. *Advances in Water Resources*, 80, 69–78.

Leuven, J.R.F.W.; Pierik, H.J.; Vegt, M.v.d.; Bouma, T.J., and Kleinhans, M.G., 2019. Sea-level-rise-induced threats depend on the size of tide-influenced estuaries worldwide. *Nature Climate Change*, 9, 986–992.

Li, C.; Huang, W., and Milan, B., 2019. Atmospheric cold front–induced exchange flows through a microtidal multi-inlet bay:

Analysis using multiple horizontal ADCPs and FVCOM simulations. *Journal of Atmospheric and Oceanic Technology*, 36, 443–472.

Li, S.; Wahl, T.; Talke, S.A.; Jay, D.A.; Orton, P.M.; Liang, X.; Wang, G., and Liu, L., 2021. Evolving tides aggravate nuisance flooding along the U.S. coastline. *Science Advances*, 7, eabe2412.

Moftakhari, H.R.; Jay, D.A.; Talke, S.A.; Kukulka, T., and Bromirski, P.D., 2013. A novel approach to flow estimation in tidal rivers. *Water Resources Research*, 49, 4817–4832.

Monsen, N.E.; Cloern, J.E.; Lucas, L.V., and Monismith, S.G., 2002. A comment on the use of flushing time, residence time, and age as transport time scales. *Limnology and Oceanography*, 47, 1545–1553.

Nerem, R.S.; Beckley, B.D.; Fasullo, J.T.; Hamlington, B.D.; Masters, D., and Mitchum, G.T., 2018. Climate-change–driven accelerated sea-level rise detected in the altimeter era. *Proceedings of the National Academy of Sciences*, 115, 2022–2025.

Nidzieko, N.J., 2010. Tidal asymmetry in estuaries with mixed semidiurnal/diurnal tides. *Journal of Geophysical Research: Oceans*, 115, C08006, 13 p.

Nienhuis, J.H.; Törnqvist, T.E.; Jankowski, K.L.; Fernandes, A.M., and Keogh, M.E., 2017. A new subsidence map for coastal Louisiana. *GSA TODAY*, 27, 2.

Nordio, G. and Fagherazzi, S., 2022. Storm surge and tidal dissipation in deltaic wetlands bordering a main channel. *Journal of Geophysical Research: Oceans*, 127, e2021JC017655.

Olhede, S.C. and Walden, A.T., 2002. Generalized Morse wavelets. *IEEE Transactions on Signal Processing*, 50, 2661–2670.

Ou, Y.; Xue, Z.G.; Li, C.; Xu, K.; White, J.R.; Bentley, S.J., and Zang, Z., 2020. A numerical investigation of salinity variations in the Barataria Estuary, Louisiana in connection with the Mississippi River and restoration activities. *Estuarine Coastal and Shelf Science*, 245, 107021.

Pareja-Roman, L.F.; Chant, R.J., and Sommerfield, C.K., 2020. Impact of historical channel deepening on tidal hydraulics in the Delaware Estuary. *Journal of Geophysical Research: Oceans*, 125, e2020JC016256.

Pawlowicz, R.; Beardsley, B., and Lentz, S., 2002. Classical tidal harmonic analysis including error estimates in MATLAB using T_TIDE. *Computers & Geosciences*, 28, 929–937.

Payandeh, A.R.; Justic, D.; Huang, H.; Mariotti, G., and Hagen, S.C., 2022. Tidal change in response to the relative sea level rise and marsh accretion in a tidally choked estuary. *Continental Shelf Research*, 234, 104642.

Pickering, M.D.; Wells, N.C.; Horsburgh, K.J., and Green, J.A.M., 2012. The impact of future sea-level rise on the European Shelf tides. *Continental Shelf Research*, 35, 1–15.

Sanks, K.M.; Shaw, J.B., and Naithani, K., 2020. Field-based estimate of the sediment deficit in coastal Louisiana. *Journal of Geophysical Research: Earth Surface*, 125, e2019JF005389.

Savenije, H.H.G.; Toffolon, M.; Haas, J., and Veling, E.J.M., 2008. Analytical description of tidal dynamics in convergent estuaries. *Journal of Geophysical Research: Oceans*, 113, C10025, 18 p.

Savenije, H.H.G. and Veling, E.J.M., 2005. Relation between tidal damping and wave celerity in estuaries. *Journal of Geophysical Research: Oceans*, 110, C04007, 10 p.

Snedden, G., 2006. River, Tidal, and Wind Interactions in a Deltaic Estuarine System. Louisiana State University and Agricultural & Mechanical College, Ph.D. dissertation, Baton Rouge, Louisana, 117 p.

Sorourian, S.; Huang, H.; Li, C.; Justic, D., and Payandeh, A.R., 2020. Wave dynamics near Barataria Bay tidal inlets during spring–summer time. *Ocean Modelling*, 147, 101553.

Spicer, P.; Huguenard, K.; Ross, L., and Rickard, L.N., 2019. High-frequency tide-surge-river interaction in estuaries: Causes and implications for coastal flooding. *Journal of Geophysical Research: Oceans*, 124, 9517–9530.

Stark, J.; Van Oyen, T.; Meire, P., and Temmerman, S., 2015. Observations of tidal and storm surge attenuation in a large tidal marsh. *Limnology and Oceanography*, 60, 1371–1381.

Sweet, W.V.; Kopp, R.E.; Weaver, C.P.; Obeysekera, J.; Horton, R.M.; Thieler, E.R., and Zervas, C., 2017. *Global and Regional Sea Level Rise Scenarios for the United States*. Silver Spring, Maryland: U.S. Department of Commerce, National Oceanic and Atmospheric Administration, National Ocean Service, and Center for Operational Oceanographic Products and Services, *NOAA Technical Report NOS CO-OPS 083*, 75 p.

Talke, S.A. and Jay, D.A., 2020. Changing tides: The role of natural and anthropogenic factors. *Annual Review of Marine Science*, 12, 121–151.

Thompson, P.R.; Widlansky, M.J.; Hamlington, B.D.; Merrifield, M.A.; Marra, J.J.; Mitchum, G.T., and Sweet, W., 2021. Rapid increases and extreme months in projections of United States high-tide flooding. *Nature Climate Change*, 11, 584–590.

Toffolon, M. and Savenije, H.H.G., 2011. Revisiting linearized one-dimensional tidal propagation. *Journal of Geophysical Research: Oceans*, 116, C07007, 13 p.

Törnqvist, T.E.; Jankowski, K.L.; Li, Y.-X., and González, J.L., 2020. Tipping points of Mississippi Delta marshes due to accelerated sea-level rise. *Science Advances*, 6, eaaz5512.

Torrence, C. and Compo, G.P., 1998. A practical guide to wavelet analysis. *Bulletin of the American Meteorological Society*, 79, 61–78.

van Maren, D.S.; Beemster, J.G.W.; Wang, Z.B.; Khan, Z.H.; Schrijvershof, R.A., and Hoitink, A.J.F., 2023. Tidal amplification and river capture in response to land reclamation in the Ganges-Brahmaputra delta. *CATENA*, 220, 106651.

van Rijn, L.C., 2011. Analytical and numerical analysis of tides and salinities in estuaries; Part I: Tidal wave propagation in convergent estuaries. *Ocean Dynamics*, 61, 1719–1741.

Wager, R.T., & E.L. Haywood III, 2024. State of Louisiana Coastal Protection and Restoration Authority (CPRA) Coastal Information Management System (CIMS) Data Dictionary. Version 2.0, pp 1–136.

Winterwerp, J.C. and Wang, Z.B., 2013. Man-induced regime shifts in small estuaries—I: Theory. *Ocean Dynamics*, 63, 1279–1292.

APPENDIX

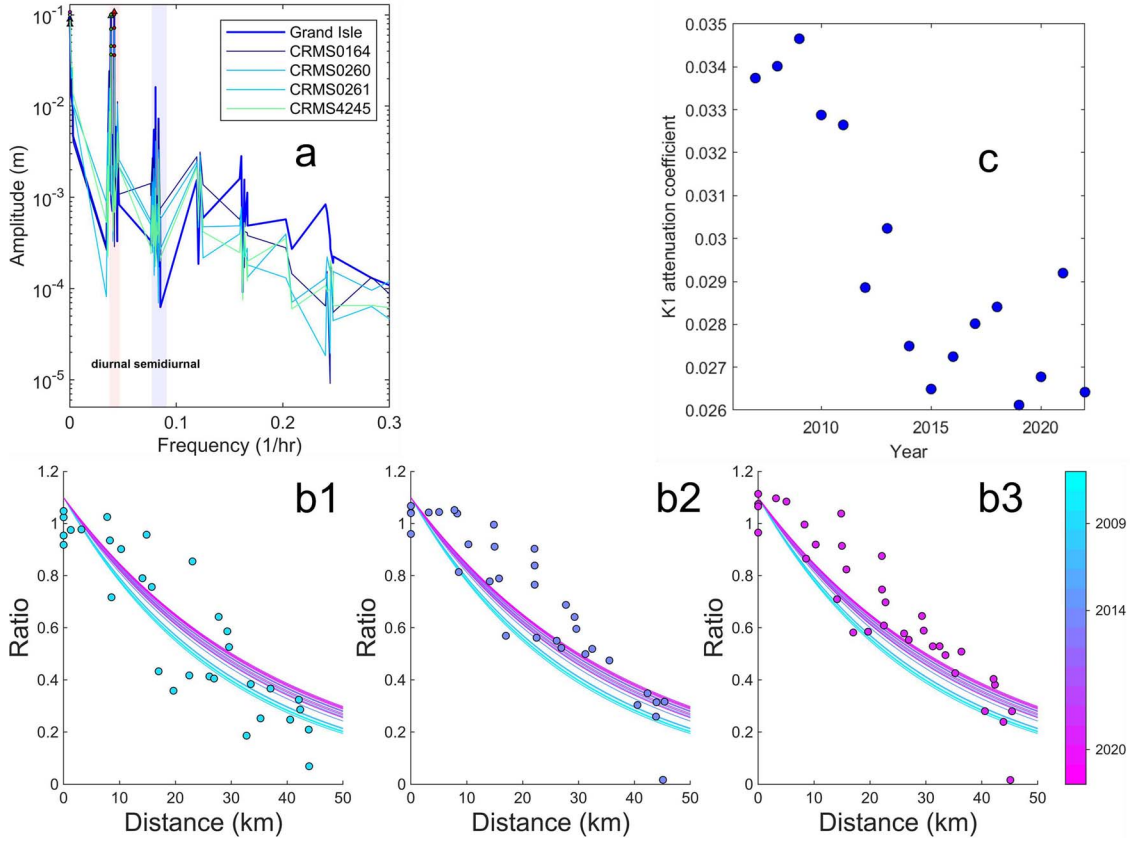

Figure A1. Tidal analysis and K1 attenuation trends. (a) Tidal spectra (lines) for Grand Isle (triangles) and an example Coastwide Reference Monitoring System (CRMS) station (circles) from January 2014 to December 2015, obtained using T-TIDE with 18.6-year nodal correction. Constituents are highlighted with colored symbols: K1 (red), O1 (green), SA (blue), and SSA (magenta). (b1–b3) K1 amplitude ratios *vs.* distance for 2009, 2014, and 2020, respectively, with identical exponential fits ($y_1 = 1.1e^{-\alpha x}$) shown for each year. (c) Yearly trend of the K1 attenuation coefficient (α).

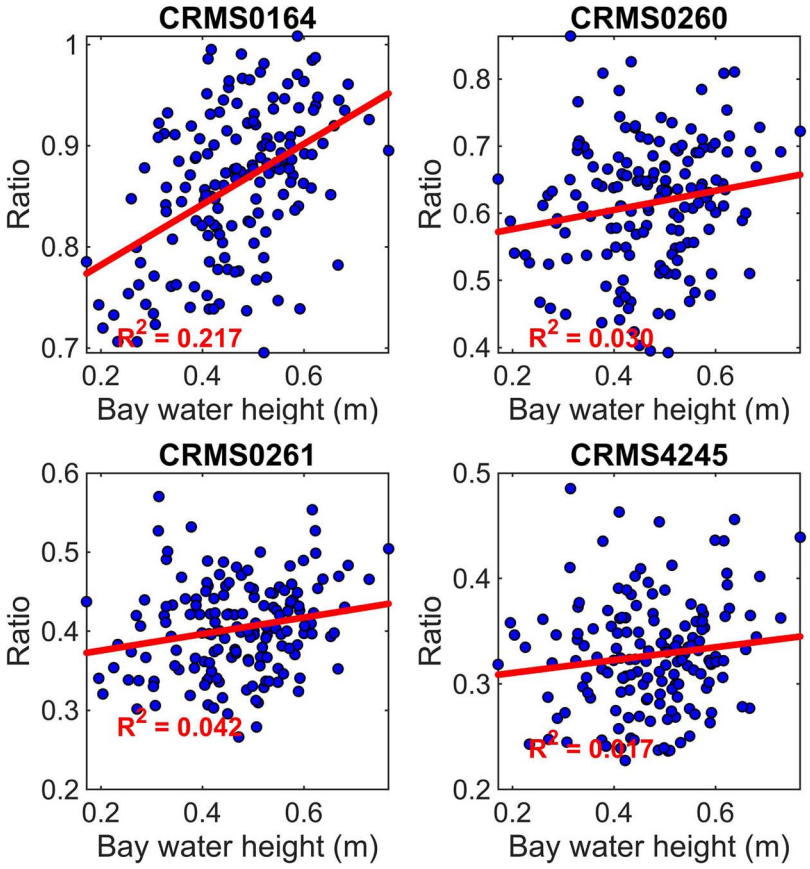

Figure A2. Correlation analysis of monthly K1 tidal constituent ratios and Barataria Bay water height. The lack of a clear linear trend suggests nonlinearity between attenuation and the sea-level change.